Investigations on the Nature of Ceramic Deposits in Plasma Spray-Physical Vapor Deposition

W. He, G. Mauer, O. Guillon, R. Vaßen, Forschungszentrum Jülich GmbH, IEK-1, Jülich / D
M. Gindrat, Oerlikon Metco AG, Wohlen / CH
R. Wäger, Helbling Technik AG, Aarau / CH

In Plasma Spray-Physical Vapor Deposition (PS-PVD) process, major fractions of the feedstock powder can be evaporated so that coatings are deposited mainly from vapor phase. In this work, Computational Fluid Dynamics (CFD) results indicate that such evaporation occurs significantly in the plasma torch nozzle and even nucleation and condensation of zirconia is highly possible there. Experimental work has been performed to investigate the nature of the deposits in the PS-PVD process, in particular coatings from condensated vapor and nano-sized clusters produced at two spraying distances of 1000 mm and 400 mm. SEM images show that, at long spraying distance, many small nano-sized particles (<20 nm) which are significantly smaller than primary particles in the feedstock powder cover the coating surface in the center of the plasma jet. However, at short spraying distance, such nano-sized particles were hardly found. Besides, in the center area of the plasma jet, XRD patterns indicate only limited preferential growth orientation at long spraying distance which might be a consequence of the low mobility of nano-sized cluster deposits. Meanwhile, at short spraying distance, XRD patterns show obvious preferred growth orientations of (110) and (002). The results give a further insight in the formation mechanisms of high quality columnar structured PS-PVD thermal barrier coatings which have already shown excellent performance in cyclic life time tests.

1   Introduction

Plasma Spray-Physical Vapor Deposition (PS-PVD) is a novel technology, named for vapor phase deposition by using plasma spraying [1]. At a very low working pressure of 50 to 200 Pa, the plasma jet is less cooled and decelerated, which leads to a plasma jet more than 2 meters in length and a diameter ranging from 200 mm to 400 mm [2]. Therefore, PS-PVD has been developed for deposition of thin and uniform coatings with large area coverage [3]. With enhanced electric input power up to 180 kW, the feedstock material even can be evaporated so that coating deposition mainly comes from vapor phase [4]. The interaction of plasma gas and vapor phase of feedstock makes non-line-of-sight deposition possible to deposit high quality columnar structured coating not only on the front side of substrate but also on the shadowed parts of substrates [5].

Currently, columnar structured thermal barrier coatings (TBCs) on aero-engines with the highest load are mainly manufactured by electron beam physical vapor deposition (EB-PVD). At PS-PVD conditions, suitable process parameters and specific feedstock powder enable manufacturing columnar structured ceramic topcoats as well. And recently, such columnar structured TBCs produced by PS-PVD have shown improved thermal cycling lifetimes more than two times higher than conventionally sprayed TBCs [6]. Moreover, the deposition rate of PS-PVD is significantly higher than that of EB-PVD, which makes PS-PVD be the most promising alternative process for depositing columnar structured TBCs. Therefore, to obtain a better understanding of deposition mechanisms of high quality columnar structured PS-PVD coatings is now a focus issue.

In the previous work, a structure zone model for magnetron sputtered coatings proposed by Thornton was transferred to PS-PVD to illustrate coating characteristics because it generally corresponds well with the characteristics of PS-PVD coatings formed by shadowing, surface diffusion, and bulk diffusion [7]. Further calculations indicated that nano-sized clusters can be formed in the boundary layer of the substrate by homogeneous nucleation and condensation from super-saturated vapors [8]. Thus, deposition in PS-PVD takes place not only from liquid splats but also from nano-sized clusters or directly from the vapor phase. In this work, Computational Fluid Dynamics (CFD) results confirm former calculations indicating that such evaporation occurs significantly in the plasma torch nozzle. Experimental work has been performed to investigate the nature of the deposits in the PS-PVD process, in particular coatings from nano-sized clusters.

2   Experimental procedures

2.1   Coating deposition

The coatings were carried out on an Oerlikon (formerly Sulzer) Metco Multicoat system, which can achieve the low working pressure of 200 Pa and a maximum input power of 150 kW. An O3CP torch was applied to generate the plasma jet with 35 slpm argon and 60 slpm helium as plasma gases plus 2x16 slpm argon carrier gas.

The feedstock powder was monoclinic zirconia agglomerated with 7 wt.% cubic yttria (YSZ) produced by Oerlikon Metco designated as M6700. The particle size distribution was about: d_{10}=6.6 μm, d_{50}=11.5 μm, d_{90}=19.0 μm.

In order to investigate the nature of vapor phase deposition in PS-PVD process, a high current of 2750 A and a low powder feed rate of 5 g/min was used in coating processes at two spraying distances of 1000 mm (test A) and 400

mm (test B). The substrate temperature (T_s) of coating at 400 mm was estimated about 2000°C, therefore graphite was utilized as substrate material in all coating processes. Spraying parameters are shown in Table 1.

Table 1. Plasma spray parameters.

Test	A	B
Spraying distance (mm)	1000	400
Plasma gas (slpm)	Ar 35 / He 60	
Current (A)	2750	
Net power (kW)	60	
Powder feed rate (g/min)	5	
Carrier gas (slpm)	2x16	
Spraying duration (min)	5	2

*slpm: standard liter per minute

In test A, the substrate temperature was recorded at two positions P1 and P2 by thermocouples (Type K) inserted into the substrate from backside. P1 is the center of plasma jet and P2 is 40 mm offset from center. During spraying, plasma torch and samples were not moved. The positions of substrate and thermocouples are shown in **Fig. 1**.
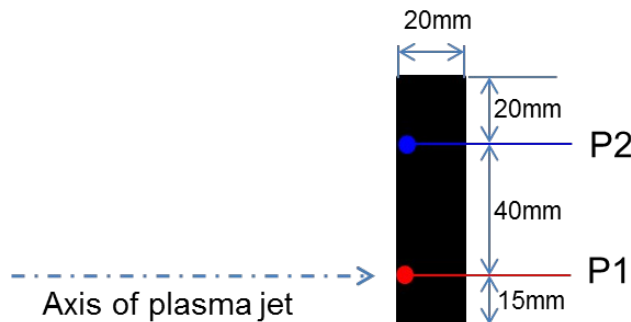

Fig. 1. Schematic drawing of positions of substrate and two thermocouples during coating in test A.

2.2   Simulation methods

CFD is the art of fluid mechanics which can solve and analyze or even provide a qualitative (and sometimes even quantitative) prediction of fluid flows by means of mathematical modeling, numerical methods, and software tools. In present work, the model and simulation were carried out with the latest version of Ansys CFX. The O3CP torch was full 360° simulated by hexahedral mesh. The outlet of the torch was set with a parabolic shaped boundary.

2.3   Characterization methods

Coating morphologies was investigated by scanning electron microscopy (SEM, Ultra 55, Zeiss - Germany) and Hitachi TM3000 tabletop microscope (Germany). X-ray diffraction (XRD, D4 Endeavor - Bruker AXS) was carried out to determine the phase composition and preferred growth orientations in the coatings.

3   Results and discussion

3.1   Computational Fluid Dynamic simulation

CFD simulation was applied to simulate the interaction of plasma and feedstock after injection. Table 2 shows some adapted material properties, boundary conditions, and parameters during spraying delivered by PS-PVD facility.
The temperature distribution in O3CP torch is shown in Fig. 2, and the highest plasma temperature is reached at the axis of torch. Particle tracks are colored by diameter. Despite that particles are not able to reach the core of plasma, the plasma temperature is much higher than vaporization temperature of zirconia. Hence, the reducing of mean particle diameter illustrates evaporation of zirconia. The simulation results show that a significant amount of zirconia feedstock, about 56.8 wt.%, has been evaporated in the nozzle.

Table 2. Constant values used for the computational simulation.

Latent heat of fusion of ZrO_2	H_{melt}= 700 kJ/kg
Latent heat of vaporization of ZrO_2	H_{evap}= 5096 kJ/kg

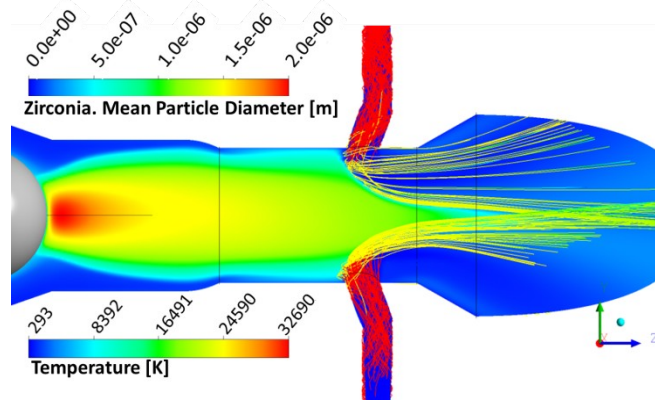| Melting temperature	T_m= 2950 K
Specific heat [9] 1) $T < 1478$ K 2) 1478 K $< T < T_m$ 3) $T_m < T$	1) c_p= 1000*(16.64 + 1.8$*10^{-3}$*T- 3.36$*10^5*T^2$) * 0.033977423 J/kg K 2) c_p= 0.605 J/kg K 3) c_p= 0.714 J/kg K
Cathode back wall temperature	T = 300K
Anode voltage	U = 50 V
Arc attachment on anode fixed (rel. to x-axis)	α = 135 deg
Plasma gas	Ar 35 slpm /He 60 slpm
Carrier gas	2x16 slpm
Carrier gas temperature	300 K
Powder (YSZ)	0.333 g/s
Current	2600 A
Voltage	48 V
Input power	124.8 kW
Net power	60 kW

Fig. 2. Plasma temperature with particle tracks colored by diameter.
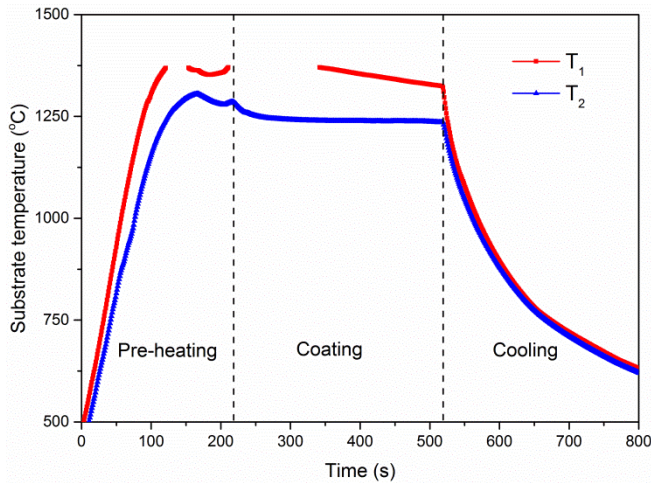
3.2   Experimental results

Fig. 3. Substrate temperature measurement in test A: T_1 and T_2 are temperatures at P1 and P2.

In test A, during spraying process, two thermocouples were used to monitor the substrate temperature at two positions: P1 the center of plasma jet and P2 the edge (40 mm offset from center) of plasma jet. Fig. 3 shows the temperature measurement results. The data loss of T_1 is because substrate temperature is out of measuring range of the thermocouple (1370°C). Before coating, the substrate was heated up to obtain a better adhesion between substrate and YSZ coating. During pre-heating, if only the heat transfer from plasma to substrate is considered, $T_1 > T_2$ means that the plasma temperature in the center is higher and it is assumed that the temperature difference between the coming plasma and substrate is the same for the whole substrate. The temperature drop during preheating is caused by current adjustment.

On coating onset, T_2 decreases a little due to the formation of thermal barrier coating. Then it keeps constant while T_1 keeps reducing until the end of coating. The result basically illustrates: T_1 is higher than 1324°C and T_2 is higher than 1235°C. Therefore, the ratio between T_s and melting point of zirconia (T_m = 2715°C), T_s/T_m, is between 0.5~0.55. Columnar structured coating was deposited on the substrate. **Fig. 4** shows a fracture surface of the coating in test A and test B. In test A, the coating A1 (**Fig. 4**A1) deposited in the center of plasma jet, a typical column starts to grow up first along the normal direction of substrate with large diameter and then branches into many finer columns. At the edge of plasma jet, coating A2 (**Fig. 4**A2) has limited thickness so that from the bottom to the top of columns show relatively uniform diameter. While in test B, the coating B1, also deposited in the center of plasma jet, shows a very high deposition rate. It reduces from A1 to A2 as well as from B1 to A1, indicating high concentration of deposition species either in the center of plasma jet or at short spraying distance. Besides, in the inset of Fig. 4A2, some micron-sized spherical particles are noticeable. Additionally, in Fig. 2, the particle tracks show that some particles do not reach the core of plasma and still keep their particle sizes at the exit of torch. These kinds of particles are not easy to be evaporated, and they will be directly solidify and incorporated in the coating.
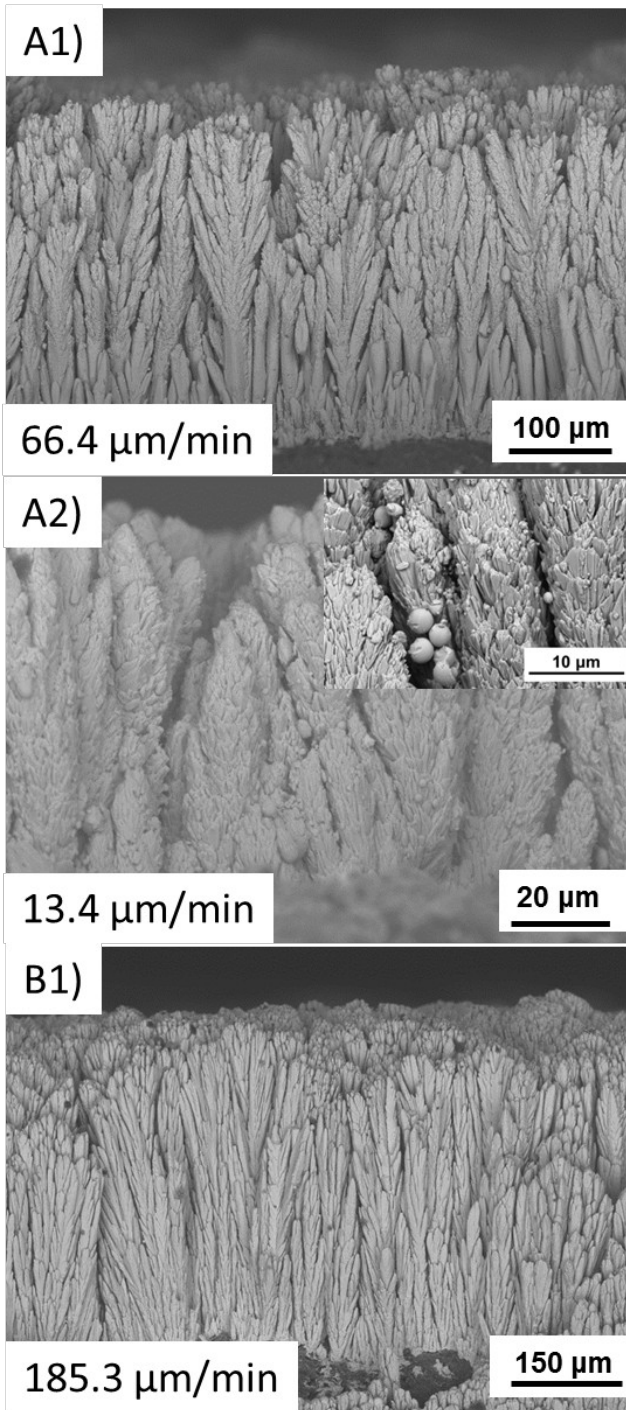
Fig. 4. SEM (back-scattered electron) images of fracture surfaces: A1), A2) and B1) are corresponding to position P1, P2 in test A (1000 mm) and P1 in test B (400 mm), respectively. An approximate growth rate in unit of µm/min is given in the images.

Fig. 6 shows the tops of columns of the coatings sprayed in test A and B. It is obvious that the coatings sprayed at 1000 mm (Fig. 6A1 and A2) have pyramid shaped top and faceted structure. But it is also visible that the faceted structure of coating A2 is not as sharp as that of coating A1. Besides, it is noteworthy that some strips and many nano-sized particles cover on every small facet of coating sprayed at 1000 mm. And the size of these particles is about or even smaller than 20 nm, which is significantly smaller than the original nano-particles in the feedstock powder (seen in Fig. 5). Hence, such kind of nano-particles must be the result of nucleation and growth of vapor phase, which could be an evidence of nano-sized cluster deposition in PS-PVD. With reducing spraying distance to 400 mm, columns in the coating B1 (Fig. 6B1) have flat tops and do not show faceted structure any more. And on the top of coating B1, nano-sized particles are not visible but some regular shaped bulges. The different microstructures of the coatings indicate different crystal growth patterns.
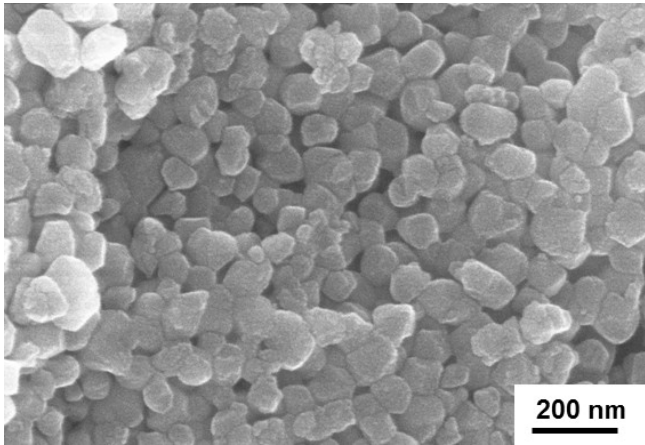
Fig. 5 SEM (secondary electron) images of original nano-sized particle in the feedstock powder.

XRD was carried out to determine the phase compositions and crystal structures of the coatings. The XRD patterns in Fig. 7 show that the main phase of coating produced by PS-PVD is tetragonal YSZ. But a small amount of monoclinic phase also exists in the coating. Because the feedstock powder is an agglomeration of monoclinic zirconia and cubic yttria (XRD pattern in Fig. 7), the monoclinic phase should come from unmelted or unevaporated feedstock powder particles as seen in Fig. 4A2. Meanwhile, major fraction of powder feedstock was evaporated so that the deposition of vapor mixture of zirconia and yttria leads to tetragonal phase at room temperature. Due to very high substrate temperature at 400 mm, small amount of ZrC formed in the coating. Comparing to coating A1, the narrower peaks in coating A2 mean larger crystallite size.

According to Rietveld analysis of the coatings (seen in Table), there is no indication of preferred orientation (PO) in coating A1. But PO of crystallographic plane (110) is found in coating A2 and coating B1 has crystallographic planes (002) and (110) as POs. Chen et al. compared that the surface free energy density of (002) is larger than that of (110) [10], which means under the same growth conditions, the growth of (110) is more thermodynamically stable than (002).
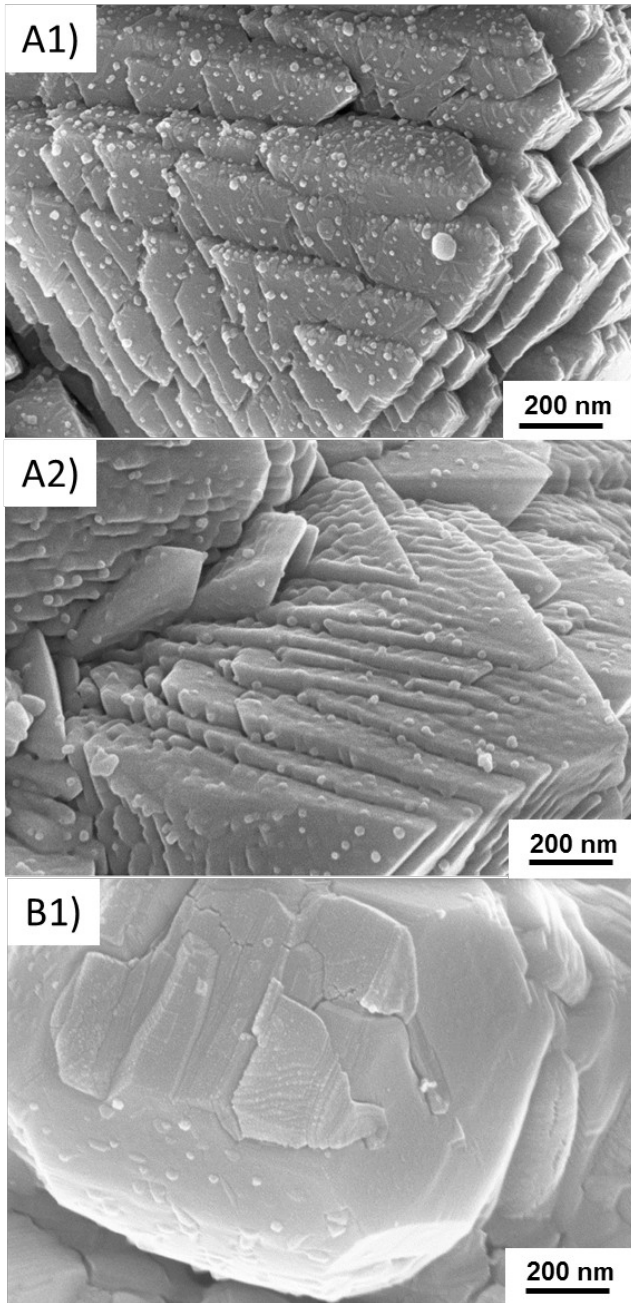
Fig. 6. SEM (secondary electron) images of column tops: A1), A2) and B1) are corresponding to position P1, P2 in test A (1000 mm) and P1 in test B (400 mm), respectively.

Table 3. Rietveld analysis of the coatings.

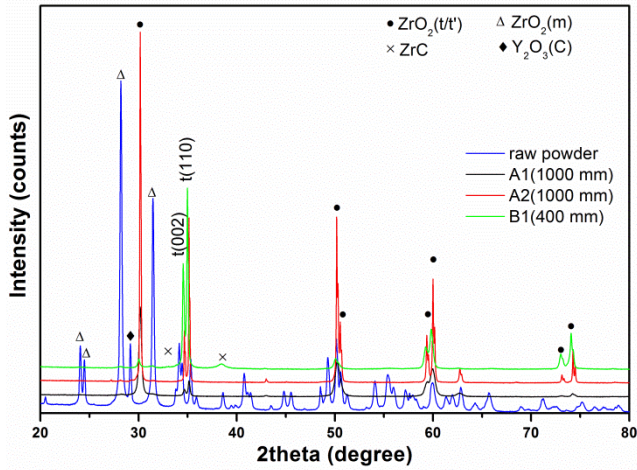| Coating	Amount of monoclinic	Preferred orientations
A1	~5%	-
A2	~3%	(110)
B1	~5%	(002) (110)

Fig. 7. XRD patterns of the raw powder and the coatings: A1), A2) and B1) are corresponding to position P1, P2 in test A (1000 mm) and P1 in test B (400 mm), respectively.

3.3   Discussion

In a previous work, a preliminary PS-PVD structure zone model (SZM) was built up to illustrate the characteristics of PS-PVD coatings formed by shadowing, surface, and bulk diffusion [7]. It is suggested that substrate temperature (relating to the activation energy) and impingement rate are two significant parameters in relation to the characteristic features of the PS-PVD coating microstructures.

According to the CFD simulation results, evaporation of YSZ occurs significantly in the nozzle. Due to large temperature gradient between the hot plasma and the cool nozzle wall, supersaturation can be achieved in the nozzle. Likewise, the temperature gradient between substrate and the coming plasma jet is also huge, which would also lead to the formation of supersaturated vapor in the boundary layer of the substrate. In a supersaturated vapor, the critical nucleus size of homogeneous nucleation for a stable nucleus can be written as [11]

$$d^{\iota} = \frac{4\sigma \upsilon_1}{k_B T \ln S} \qquad \text{(Equ. 1)}$$

wherein σ is the surface tension, υ_1 is the monomer volume, k_B is the Boltzmann constant, T is the absolute temperature, S is the supersaturation ratio which is defined as n_1/n_s (n_1 is the concentration (m^{-3}) of monomer, n_s is the equilibrium monomer concentration). Once the S >1, a minimum diameter for nucleation can be achieved. Therefore, the formation of nano-sized clusters in the boundary layer should also be taken into consideration.

According to S. L. Girshick's calculation [12], the nucleation burst is followed by steady growth by coagulation and the particle size distributions are broadened by non-uniform temperature, velocity profiles, and by particle deposition to substrates. The study also pointed out that the size and number of nucleated particles can be significantly affected by two factors, the cooling rate at the location of nucleation and the monomer concentration n_1 (assumed only one condensable species in vapor). Lower local cooling rates and higher concentrations both favor the nucleation of larger (and fewer) particles.

In present work, a higher concentration of deposition species in the center of plasma jet was demonstrated by the higher deposition rate. And from the temperature measurement result, at the same spraying distance an almost same cooling rate can be expected for the vapor species. Therefore, in the center of plasma jet (P1), higher concentration of deposition species will lead to formation of larger and fewer clusters.

A previous report gives experimental evidences for cluster deposition shows that the mobility of the particles strongly decreases as their size increases [13]. In other words, larger sized cluster will have higher activation energy.

At spraying distance of 1000 mm, even though the substrate temperature at P1 was higher than at P2, due to the formation of large size clusters at P1, the mobility of the clusters are inhibited and therefore they are difficult to move to each other on the substrate surface, which can be confirmed by the absence of preferred orientation. While at P2, the relatively smaller clusters are able to diffuse on the substrate surface to find a low Gibbs' energy spots to build up coating with preferred orientation of (110). And due to the diffusion of clusters, they could have chance to coalesce with each other to grow as large crystallites.

If the spraying distance is reduced to 400 mm, the substrate temperature is estimated around 2000°C. T_s/T_m is about between 0.7~0.75. The very high concentration of deposition species will lead to larger clusters, which could result in high difficulty of clusters mobility. However, due to the extremely high substrate temperature, surface diffusion or even bulk diffusion possibly occurs so that the coating B1 shows preferred orientation of (110) and (002). The growth of (002) crystal plane must be the reason for the flat column top (Fig. 6B1).
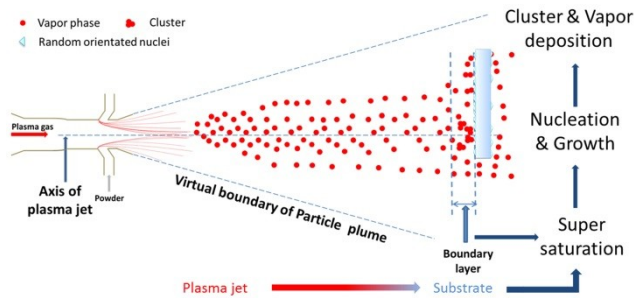
Fig. 8 Schematic drawing of the proposed cluster and vapor deposition in PS-PVD.

According to the above analysis, a proposed coating build-up of vapor and cluster deposition in PS-PVD is depicted schematically in Fig. 8. From the exit of plasma torch, the shape of particle plume is divergent, therefore high concentration of deposition species can be expected in the center of the plasma jet. In the chamber, the plasma jet is laminar and the interaction of the plasma jet with the surrounding atmosphere is weak [14]. Therefore, the plasma jet is less the plasma jet is less cooled and decelerated. As the hot plasma jet comes close to the relatively cool substrate, a boundary layer is formed due to the rapidly decreasing of temperature and velocity. In the boundary layer, homogeneous nucleation can form nano-sized clusters as a result of supersaturation of vapor species. The size of clusters is mainly dependent on the local concentration of vapor species and also influenced by cooling rate. At the same time, heterogeneous nucleation of vapor species can occur also directly on the substrate. Both the homogeneous nucleation and the heterogeneous nucleation contribute to the coating deposition. Further build-up of coating is mainly governed by the substrate temperature. In summary, the coating produced by PS-PVD is a mixture of cluster and vapor deposition.

4   Conclusions

In this work, CFD simulation for the O3CP torch gives indication of significant evaporation of YSZ already in the plasma torch. Columnar structured TBCs were successfully manufactured by PS-PVD. The microstructures and morphologies of the different areas of the coatings show formation of nano-sized particles on the top of columns. Preferred orientations of the coatings were investigated, which gives an explanation to the different microstructures of the coatings.
Based on the results, a cluster deposition in PS-PVD was proposed. The huge temperature gradient from hot plasma to cool substrate results in supersaturation of vapor phase formed in the boundary layer of substrate. Homogeneous nucleation of vapor species can occur in the boundary layer forming clusters while heterogeneous nucleation of vapor species could also occur directly on the substrate. After the clusters and vapor species impact on the substrate surface, the build-up of coating is significantly influenced by substrate temperature.

5   Acknowledgements

6   Literature

[1] Von Niessen, K., M. Gindrat, and A. Refke. Vapor phase deposition using plasma spray-PVD™. Journal of thermal spray technology 19 (2010), Issue 1-2, pp. 502/09.
[2] Goral, Marek, Slawomir Kotowski, and Jan Sieniawski. The Technology of Plasma Spray Physical Vapour Deposition. High Temperature Materials and Processes 32 (2013), Issue 1, pp. 33/39.
[3] Hospach, A., et al. Columnar-structured thermal barrier coatings (TBCs) by thin film low-pressure plasma spraying (LPPS-TF). Journal of thermal spray technology 20 (2011), Issue 1-2, pp. 116/20.
[4] Mauer, G., et al. Novel opportunities for thermal spray by PS-PVD. Surface and coatings technology 268 (2015), pp. 52/57.
[5] Mauer, G., Robert V., and Detlev S. Thin and dense ceramic coatings by plasma spraying at very low pressure. Journal of thermal spray technology 19 (2010), Issue 1-2, pp. 495/501.
[6] Rezanka S., Mauer G., and Vaßen R. Improved thermal cycling durability of thermal barrier coatings manufactured by PS-PVD. Journal of Thermal Spray Technology 23 (2014), Issue 1-2, pp. 182/89.
[7] Mauer, G., et al. Process conditions and microstructures of ceramic coatings by gas phase deposition based on plasma spraying. Journal of thermal spray technology 22 (2013), Issue 2-3, pp. 83/89.
[8] Mauer, G., Rezanka, S. Hospach, A., Vaßen, R. and Guillon, O. The Role of Nucleation and Growth in Plasma Spray-Physical Vapor Deposition, to be published in Plasma Chem. Plasma Proc. 2016.

[9] Chase, M.W. Jr., Davies, C.A., Downey, J.R. Jr., Frurip, D.J., McDonald, R.A., Syverud, A.N., NIST-JANAF Themochemical Tables, Fourth Edition, J. Phys. Chem. Ref. Data, Monograph 9, National Institute of Standards and Technology, Gaithersburg, MD., 1998, pp. 1/1951.

[10] Chih-Chiang, C. et al. Growth of zirconia and yttria-stabilized zirconia nanorod arrays assisted by phase transition. CrystEngComm 12 (2010), Issue 11, pp. 3664/69.

[11] Thomson, W. 4. On the Equilibrium of Vapour at a Curved Surface of Liquid. Proceedings of the Royal Society of Edinburgh 7 (1872), pp. 63/68.

[12] Girshick, S. L., and C-P. Chiu. Homogeneous nucleation of particles from the vapor phase in thermal plasma synthesis. Plasma Chemistry and Plasma Processing 9 (1989), Issue 3, pp. 355/69.

[13] Melinon, P. et al. Comparison of molecular and cluster deposition: Evidence of different percolation processes. Physical Review B 44 (1991), Issue 22, pp. 12562.

[14] Mauer, G. Plasma Characteristics and Plasma-Feedstock Interaction Under PS-PVD Process Conditions. Plasma Chemistry and Plasma Processing 34 (2014), Issue 5, pp. 1171/86.